Applied Surface Science 342 (2015) 174–182

Contents lists available at ScienceDirect

Applied Surface Science

journal homepage: www.elsevier.com/locate/apsusc

The selective catalytic reduction of NO with NH_3 over a novel Ce–Sn–Ti mixed oxides catalyst: Promotional effect of SnO_2

Ming'e Yu[a,b], Caiting Li[a,b,*], Guangming Zeng[a,b], Yang Zhou[a,b], Xunan Zhang[a,b], Yin'e Xie[a,b]

[a] College of Environmental Science and Engineering, Hunan University, Changsha 410082, PR China
[b] Key Laboratory of Environmental Biology and Pollution Control (Hunan University), Ministry of Education, Changsha 410082, PR China

ARTICLE INFO

Article history:
Received 1 January 2015
Received in revised form 9 March 2015
Accepted 10 March 2015
Available online 18 March 2015

Keywords:
SCR
NH_3
Ce–Sn–Ti mixed oxides catalyst
NO removal efficiency
Reaction mechanism

ABSTRACT

A series of novel catalysts (CexSny) for the selective catalytic reduction of NO by NH_3 were prepared by the inverse co-precipitation method. The aim of this novel design was to improve the NO removal efficiency of CeTi by the introduction of SnO_2. It was found that the Ce–Sn–Ti catalyst was much more active than Ce–Ti and the best Ce:Sn molar ratio was 2:1. Ce2Sn1 possessed a satisfied NO removal efficiency at low temperature (160–280 °C), while over 90% NO removal efficiency maintained in the temperature range of 280–400 °C at the gas hourly space velocity (GHSV) of 50,000 h^{-1}. Besides, Ce2Sn1 kept a stable NO removal efficiency within a wide range of GHSV and a long period of reacting time. Meanwhile, Ce2Sn1 exhibited remarkable resistance to both respectively and simultaneously H_2O and SO_2 poisoning due to the introduction of SnO_2. The promotional effect of SnO_2 was studied by N_2 adsorption–desorption, X-ray diffraction (XRD), Raman spectra, X-ray photoelectron spectroscopy (XPS) and H_2 temperature programmed reduction (H_2-TPR) for detail information. The characterization results revealed that the excellent catalytic performance of Ce2Sn1 was associated with the higher specific surface area, larger pore volume and poorer crystallization. Besides, the introduction of SnO_2 could result in not only greater conversion of Ce^{4+} to Ce^{3+} but also the increase amount of chemisorbed oxygen, which are beneficial to improve the SCR activity. More importantly, a novel peak appearing at lower temperatures through the new redox equilibrium of $2Ce^{4+} + Sn^{2+} \leftrightarrow 2Ce^{3+} + Sn^{4+}$ and higher total H_2 consumption can be obtained by the addition of SnO_2. Finally, the possible reaction mechanism of the selective catalytic reduction over Ce2Sn1 was also proposed.

1. Introduction

Nitrogen oxides (NO, NO_2 and N_2O), which are originated from both diesel engine exhaust and stationary power plants, can not only cause the photochemical smog and acid rain, but also contribute to the ozone depletion and greenhouse effect [1–3]. Consequently, the elimination of nitrogen oxides has become a research hotspot in recent years and several potential denitrification techniques have been employed. Among the flue gas treatment methods, selective catalytic reduction (SCR) with ammonia in the presence of excess oxygen is regarded as the most chemical effective and economical post-combustion technology for the abatement of nitrogen oxides [2,4,5].

As the core ingredient of SCR, a number of catalysts have been extensively investigated. The anatase TiO_2 supported V_2O_5–WO_3 or V_2O_5–MoO_3 has been adopted worldwide in practice for decades due to its excellent catalytic performance and high resistance to SO_2 in the SCR reaction within the temperature range of 300–400 °C [6,7]. In spite of its widespread application, there still remain some inevitable disadvantages restrained the practical applications, such as: the biological toxicity of vanadium species, the narrow temperature operation window, the high activity for the oxidation of SO_2 to SO_3 and the low N_2 selectivity at high temperature due to the formation of N_2O [6,8]. Hence, it is desirable and necessary to develop novel SCR catalysts with merits of non-toxicity and high catalytic performance.

It has been reported that numerous catalysts consisted of various mental oxides, such as Mn, Ce, Fe and Cu loaded on different supports, exhibited a variety of catalytic activities under different reaction conditions [9–11]. Among them, ceria attracted much attention spontaneously due to the considerable oxygen storage capacity and the outstanding redox ability derived from the

* Corresponding author at: College of Environmental Science and Engineering, Hunan University, Changsha 410082, PR China. Tel.: +86 731 88649216; fax: +86 731 88649216.
E-mail addresses: ctli@hnu.edu.cn, ctli3@yahoo.com (C. Li).

http://dx.doi.org/10.1016/j.apsusc.2015.03.052
0169-4332/

shift between Ce^{4+} and Ce^{3+} [12,13]. Consequently, Ce-based catalysts have been extensively studied, such as Ce–carbon oxides [14], Ce–Al [15], Mn–Ce [16], Ce–Ni [12], Ce–V [17] and so on. Herein, ceria supported on titania seems to be a promising candidate and mostly studied for the SCR. Researchers reported that the CeO_2/TiO_2 catalysts prepared by different methods displayed a high SCR catalytic activity, an excellent selectivity to N_2, broad operation temperature window and remarkable resistance to space velocity [18–20]. Besides, the introduction of different metal oxides involving Cu, W, Mo and F to CeO_2/TiO_2 are conductive to enhancing SCR activity and preventing the deactivation by SO_2 and H_2O through the strong interaction between Ce and different metal oxides [13,21–23].

SnO_2 has been widely used as an oxidation catalyst because it can reversibly undergo between Sn^{4+} and Sn^{2+} at relatively low temperatures [24]. Generally, SnO_2 can oxidize chemisorbed CO through lattice oxygen release with the participation of surface oxygen vacancies formed at temperatures lower than 227 °C [25,26]. Alternatively, SnO_2 can be also used and functions well as a promoter in spite of its minor application in SCR. Li et al. reported that Ce–Sn mixed oxides exhibited good catalytic activity in a broad temperature range from 100 °C to 400 °C at the space velocity of 20,000 h^{-1} [27]. It was also found that Sn modified MnO_x–CeO_2 catalysts exhibited nearly 100% NO conversion at temperatures of 110–230 °C with a Sn:Ce:Mn = 1:4:5 molar ratio and showed remarkably improved tolerance to SO_2 [28,29].

For the reasons and researches above, we put forward the idea to employ SnO_2 to modify CeTi catalyst, which is bound to exhibit excellent catalytic performance for SCR reaction and remarkable resistance performance to SO_2 and H_2O. In the present work, novel Ce–Sn–Ti catalysts containing different amounts of Sn were prepared by the inverse co-precipitation method. The effects of SnO_2 additive on the catalytic performance and the influence of SO_2 and H_2O were systematically investigated, taking into account the characterization results by N_2 adsorption–desorption, X-ray diffraction (XRD), Raman spectra, X-ray photoelectron spectroscopy analysis (XPS) and H_2 temperature programmed reduction (H_2-TPR).

2. Experimental

2.1. Preparation of catalysts

All the catalysts were synthesized by the inverse co-precipitation method using $Ce(NO_3)_3{\cdot}6H_2O$, $SnCl_4{\cdot}5H_2O$, $Ti(SO_4)_2$ as precursors and $NH_3{\cdot}H_2O$ as precipitator. The process was described as follows. Firstly, the desired amounts of precursors were added into deionized water with continuously magnetic stirring for an hour until completely dissolved and homogeneous mixing. Later, the solution was slowly added into the excess ammonia under vigorously stirring at room temperature until the PH of the solution reached 10 and kept stirring for another 3 h. The resulting suspension was aged in air for 48 h, followed by subsequent filtration and washed several times with deionized water until the filtrate was neutral. After that, the obtained cake was oven dried 105 °C for 12 h and finally calcined at 500 °C in a muffle furnace for 6 h. Lastly, all the samples were grinded and sieved to 60–80 mesh. The molar ratio of Ce/Ti was fixed at 1:4, while the molar ratio of Ce/Sn set four values 4:1, 2:1, 1:1, and 1:2. These synthesized samples were donated as Ce*x*Sn*y*, for example, Ce4Sn1 represented that the mole ratio of Ce:Sn is 4:1. In addition, Sn–Ti mixed oxides were prepared by a similar way for comparison and the molar ratio of Sn/Ti was determined by the best loading proportion of Sn in the Ce–Sn–Ti mixed oxides, donating as SnTi.

2.2. Activity tests of catalysts

The SCR activity tests of these synthesized samples for the selective catalytic reduction of NO by NH_3 in the presence of excess oxygen were performed in a fixed bed quartz reactor consisting of a vertical tube (20 mm nominal ID × 406.4 mm long) and a three-zone temperature controlled furnace. In each test, 500 mg sample was used and the reaction temperature ranged from 80 °C to 400 °C.

The standard simulated flue gas was composed of 800 ppm NO, 800 ppm NH_3, 5% O_2, 200 ppm SO_2 (when used), and N_2 in balance, controlled accurately by a set of mass flow controllers. The total flow rate was kept at 500 ml/min, corresponding to a gas hourly space velocity (GHSV) of approximately 50,000 h^{-1}. 5% H_2O vapor (when used) was generated by using a peristaltic pump to transfer water into the stainless steel tube wrapped with a temperature-controlled heating line and then the heated N_2 took the H_2O vapor along with the flue gas. Before entering the reactor, reactant gases were mixed in a gas mixing tank.

The concentrations of NO, NO_2, and SO_2 in the inlet and outlet were analyzed by a flue gas analyzer (Kane 950, Kane Corp., UK). The NO removal efficiency was calculated according to the following equation:

$$\text{NO removal efficiency } (\%) = \frac{[NO]_{in} - [NO]_{out}}{[NO]_{in}} \times 100\% \quad (1)$$

where $[NO]_{in}$ stands for the inlet NO concentration (ppm) and $[NO]_{out}$ presents the outlet NO concentration (ppm).

2.3. Characterizations of catalysts

The BET specific surface areas and BJH pore size distribution were measured by nitrogen adsorption–desorption using a Micromeritics ASAP 2020 M+C volumetric sorption analyzer (Micromeritics Instrument Corp., USA) at −196 °C. Each sample was degassed at 200 °C for 5 h in vacuum before the isotherms were measured by standard nitrogen adsorption. The specific surface areas were determined by the BET (Brunauer–Emmett–Teller) method, while the pore size distributions were calculated by the BJH (Barrett–Joyner–Halenda) formula from the desorption branches of N_2 adsorption isotherm.

The X-ray diffraction (XRD) experiments were performed on Rotaflex D/Max-C power diffractometer (Rigaku, Japan) to examine the crystallinity and dispersity of the components in the catalysts. Nickel-filtered Cu target *K*α radiation (λ = 0.1543 nm) was employed and the X-ray tube was operated at 40 kV, 40 mA. The X-ray powder diffractogram was recorded at 0.02° intervals in the range of 10–80°, with a scanning speed of 0.2 s.

Raman spectra were collected on an invia-reflex laser Raman Spectrometer (Renishaw, UK) using Ar^+ laser beam at room temperature and atmospheric pressure. The Raman spectra were recorded at an excitation wavelength of 632.8 nm. The wavenumber values are accurate to 1 cm^{-1} from 100 to 1000 cm^{-1}. All samples were analyzed without any pretreatment.

The X-ray photoelectron spectroscopy (XPS) experiments were carried out on a K-Alpha 1063 X-ray photoelectron spectrometer (Thermo Fisher Scientific, USA) at room temperature, using Al *K*α radiation from micro-aggregation monochromator operating at an accelerating power of 72 W. The sample charging effects were compensated by calibrating all binding energies (BE) with the adventitious C 1s peak at 284.6 eV. An instrument error of ±0.1 eV can be assumed for the measurement.

H_2 temperature programmed reduction (H_2-TPR) profiles were obtained on a Tianjin XQ TP5080 auto-adsorption apparatus using 50 mg samples. Before the experiments, the sample was pretreated at 300 °C under nitrogen flow for 2 h (50 ml/min) and cooled to room temperature. Then the feeding gas was switched to 5% H_2/Ar

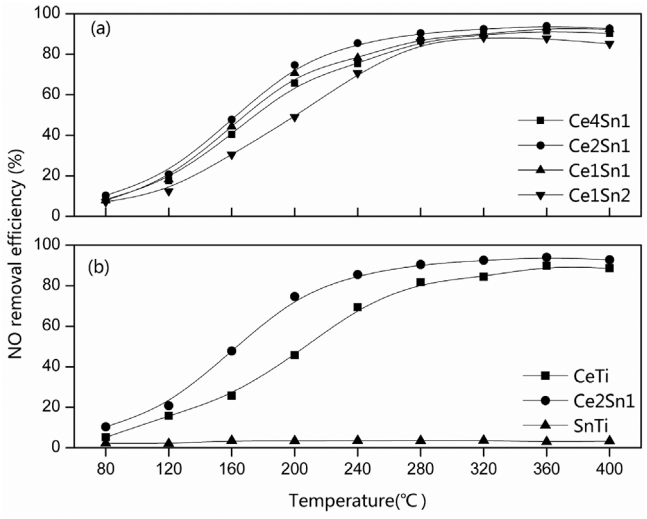

Fig. 1. NO removal efficiency over different catalysts as a function of temperature: (a) different CexSny catalysts and (b) Ce–Sn–Ti dual component oxide catalysts.

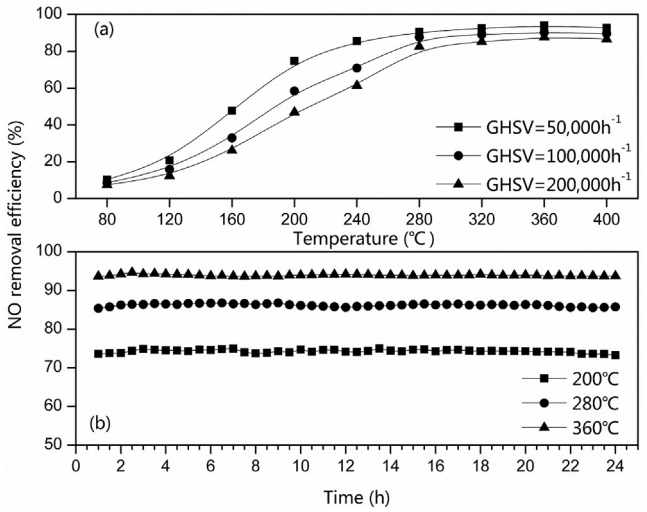

Fig. 2. The effects of different GHSV on NO removal efficiency of Ce2Sn1 (a) and the catalytic stability of Ce2Sn1 at different temperatures (b).

(50 ml/min), and the samples were heated from 100 °C to 800 °C at a ramping rate of 10 °C/min^{-1}. The hydrogen consumption was monitored quantitatively by a TCD detector.

3. Results and discussion

3.1. Catalytic activity

3.1.1. Effect of SnO_2 loading molar ratio

To find out the optimal SnO_2 loading, the NO removal efficiencies versus reaction temperature over various catalysts were shown in Fig. 1(a). It can be observed clearly that all the catalysts displayed a gradual increase in NO removal efficiency in the whole temperature. Generally, the CeTi catalyst displayed the lowest NO removal efficiency among the tested catalysts. With the increase of SnO_2 loading molar ratio from 4:1 to 2:1, the low temperature NO removal efficiency increased and the temperature range were widened, while the high temperature NO removal efficiency was maintained above 90%. However, further increasing the loading molar ratio of SnO_2 to 1:1 and 1:2 resulted in a decline in NO removal efficiency in both the low temperature range and the high temperature range. Previous researches have also demonstrated that there is always an optimal loading for the active component. When the loading of the active component increased beyond a certain value, sintering would take place on the surface of the catalysts and result in the formation of crystallization, thereby lowering the activity [30]. In summary, the CexSny catalyst possessed the best SCR catalytic performance with Ce:Sn molar ratio being 2:1, with over 90% NO removal efficiency maintaining at 280–400 °C. Compared with the traditional catalyst for the industrial formulations V_2O_5–$WO_3(MoO_3)/TiO_2$, the temperature operation window of which is 300–400 °C, Ce2Sn1 expanded the reaction temperature window and showed rather better performance (>80%) in the temperature range 200–280 °C.

Fig. 1(b) displayed the NO removal efficiencies of tri-components catalyst (Ce2Sn1) and bi-components catalysts (CeTi and SnTi). We could see from Fig. 1(b) that the activity of SnTi was rather poor and unchanged with the elevation of temperature, indicating the interaction of Sn and Ti was extremely weak. On the contrary, the NO removal efficiency of CeTi was obviously better than SnTi because of the electron interaction between Ti^{4+} and Ce^{4+}. The optimal activity of CeTi was in the temperature range of 300–360 °C, which is consistent with the literature [13,18]. The activity of the tri-components catalyst was remarkably higher than those of the bi-components catalysts, concluding that the introduction of SnO_2 had a positive influence on the SCR activity of CeTi. In spite of the superiority of Ce2Sn1, the activity of the tri-components catalyst was not a straightforward sum of the activities of the bi-components catalysts, demonstrating an interaction among the mixed oxides in Ce2Sn1. There existed two reasonable reasons: on one hand, the introduction of SnO_2 enhanced the interaction between Ti^{4+} and Ce^{4+}; on the other hand, a novel synergistic effect for the SCR reaction might exist between Sn and Ce.

3.1.2. Effect of GHSV and stability test

Considering that NH_3-SCR catalyst usually experiences different GHSV in practical application, the effect of GHSV on NO removal efficiency over Ce2Sn1 catalyst was investigated and the results were shown in Fig. 2(a). It can be seen obviously the low temperature NO removal efficiency of the catalyst decreased to some extent with increasing GHSV, while the increase of GHSV had a little influence on high temperature SCR activity, evidenced by the more than 85% NO removal efficiency from 320 °C to 400 °C even under a rather high GHSV of 200,000 h^{-1}. On the other hand, although the low temperature NO removal efficiency of the catalyst decreased to some extent with increasing GHSV, it still exhibited an excellent catalytic performance in a wide temperature range. These indicated that the Ce2Sn1 catalyst could keep stable NO removal efficiency within a wide range of GHSV, which is beneficial for its practical use.

The stability of Ce2Sn1 was also measured at 200 °C, 280 °C and 360 °C under a GHSV of 50,000 h^{-1} in Fig. 2(b). Obviously, there was almost no drastically decline in the NO removal efficiencies at different temperatures after exposed in the flue gas for 24 h, indicating a fine stability of Ce2Sn1. However, it was non-ignorable that all the efficiencies deteriorated a little and a continuous decrease could be expected because the ammonium nitrate or other by products generating in the reaction would be deposited on the active sites to damage the catalytic activity with time went by.

3.1.3. Effect of H_2O and SO_2

Water vapor and SO_2 are participators in the flue gas and difficult to remove completely, the existent of which always bring a deactivation effect to the de-nitrogen catalysis. Thus, we conducted experiments to investigate the effect of H_2O (5%) and SO_2 (200 ppm).

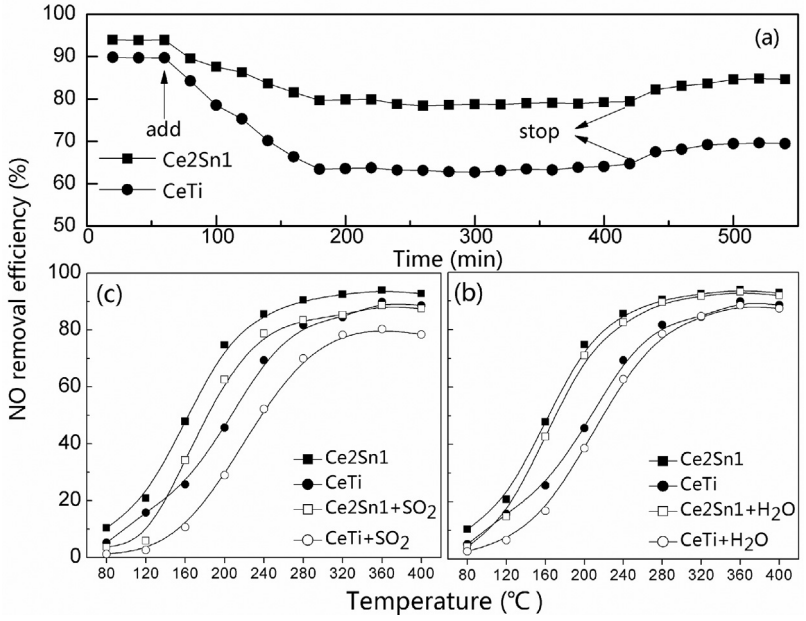

Fig. 3. (a) The synergic effect of H_2O and SO_2 on the NO removal efficiency as a function of reaction time at 360 °C. (b) Effect of individual H_2O on the NO removal efficiency over CeTi and Ce2Sn1 catalysts as a function of temperature. (c) Effect of individual SO_2 on the NO removal efficiency over CeTi and Ce2Sn1 catalysts as a function of temperature.

The synergic effect of H_2O and SO_2 on the NO removal efficiency as a function of reaction time at 360 °C was evaluated in the present work and the corresponding results were presented in Fig. 3(a). At the beginning time, both Ce2Sn1 and CeTi illustrated a normal NO removal efficiency. When H_2O and SO_2 were introduced simultaneously into the catalytic reaction system, the NO removal efficiency started to decrease firstly and a significant drop could be observed in a short time, indicating the co-existing of H_2O and SO_2 had a great influence on the NO removal efficiency. After reacting for about 2 h, the NO removal efficiency achieved a stable state and no obvious change could be observed in the following hours, which is similar with the results of other literature. Upon eliminating H_2O and SO_2 from the feed gas, the NO removal efficiency could recover to some extent, but was still lower than the initial value, representing an irreversible deactivation effect of H_2O and SO_2. Calculated from Fig. 3(a), we could obtain that the loss activity of Ce2Sn1 was about 6.7% (94–87.7%) and the NO removal efficiency of CeTi descended 22.7% (89.9–69.5%), indicating Ce2Sn1 was less influenced by co-existing of H_2O and SO_2.

The effect of individual H_2O on Ce2Sn1 and CeTi as a function of reaction temperature was also tested. At every temperature, the outlet NO concentration was recorded after reacting for 2 h and the results were shown in Fig. 3(b). In general, the existent of 5% water vapor showed a visible NO removal efficiency decreases below 280 °C for both catalysts. The inhibition effect of H_2O weakened with increasing reaction temperature and could be negligible when the reaction temperatures were higher than 280 °C. The hindering effect of water vapor at low temperatures was mainly attributed to the competitive adsorption of H_2O with reactant for the same active sites [6,13]. The effect of individual SO_2 was also tested in Fig. 3(c). A dramatically decline removal efficiency could be observed obviously within the whole temperature range. Similarly, the degree of SO_2 deactivation was dependent on the reaction temperature. The higher the reaction temperature, the less slightly the catalytic activity decreased. The deceased activity was related to formation and deposition of sulfates and sulfites on the catalyst active sites [16]. Besides, it was not difficult to find out that Ce2Sn1 presented a slighter decrease caused by both respectively and simultaneously H_2O and SO_2 than CeTi.

Based on these above results, it can be concluded distinctly that the reason for the better H_2O and SO_2 tolerance of the Ce–Sn–Ti mixed oxides catalyst might mainly lie in the participation of SnO_2. On one hand, the introduction of SnO_2 may relieve the competitive adsorption between H_2O and reactant at low temperatures. On the other hand, Xu et al. indicated that the reason for the deactivation of the CeTi catalyst is the formation of high thermally stable $Ce(SO_4)_2$ and $Ce_2(SO_4)_3$, further resulting in the disruption of the redox properties between Ce^{3+} and Ce^{4+} and the inhibition of the formation and adsorption of nitrate species [31]. Once SnO_2 was added into CeTi, not only the formation of $Ti(SO_4)_2$, $Ce(SO_4)_2$ and $Ce_2(SO_4)_3$ were prevented, but also the depositions of $(NH_4)_2SO_4$ and NH_4HSO_4 were significantly inhibited. Therefore, the Ce–Sn–Ti mixed oxides catalysts exhibited remarkable resistance to both respectively and simultaneously H_2O and SO_2 poisoning.

3.2. Characterization of catalysts

3.2.1. Structural properties (BET, XRD and LRS)

Physical properties are very important factors for catalysts to influence the adsorption–desorption behaviors of gases onto surface. Table 1 summarized the BET specific areas, BJH pore volumes and average pore diameters of CeTi, Ce2Sn1 and SnTi. As can be seen from Table 1, the tri-components catalyst Ce2Sn1 exhibited a BET specific area of 139.44 m^2/g and a pore volume of 0.5211 cm^3/g, which were found interestingly to be higher and larger than those of bi-components catalysts CeTi and SnTi. According to the results of XRD, the synergistic effect existing among the mixed oxides in the tri-components catalyst possibly restrained the crystal formation of TiO_2 in CeTi and SnTi, which may improve the BET surface area effectively [32]. There have been articles reporting

Table 1
The BET surface area, BJH pore volume and average pore width of the samples.

Samples	BET surface area (m^2/g)	BJH pore volume (cm^3/g)	Average pore width (nm)
CeTi	108.47	0.4035	9.11
SnTi	59.45	0.2724	14.12
Ce2Sn1	139.44	0.5211	11.35

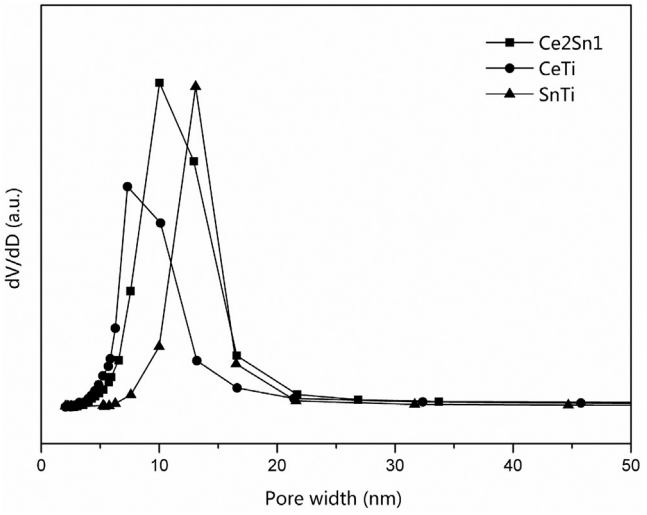

Fig. 4. The BJH pore distribution curves of SnTi, CeTi and Ce2Sn1 catalysts.

that higher surface area and larger pore volume could benefit efficient mass transfer by providing more active sites for adsorption of reactant molecules and intermediates, consequently improving the catalytic performance, which might be a reason for the superiority of Ce2Sn1 [33]. Furthermore, the pore size distribution curves measured by BJH method from desorption branch of the corresponding isotherms were shown in Fig. 4. The main pore sizes of these catalysts were distributed from 0 nm to 10 nm, belonging to the size of a mesopore, the presence of which would make a great contribution to the high BET surface area [34].

The power X-ray diffraction (XRD) was carried out to investigate the phase structures of the catalysts and the relevant results were displayed in Fig. 5. For CeTi, only the anatase TiO_2 peak at 27.5° was detected without extra characteristic diffraction peaks assigned to cubic fluorite CeO_2, which was similar with the results reported by other researchers [35,36]. The reason may lie in that CeO_2 exited as an amorphous phase in the bulk of TiO_2 crystallite or the particles were too small to be detected by XRD [20,37]. In the pattern of SnTi catalyst, the diffraction peaks attributed to SnO_2 were not shown because of the low loading ratio and the rutile TiO_2 phases were observed, which is responsible for the smaller BET surface area and the poorer catalytic activity of SnTi [6]. Compared with the bi-components catalysts, the XRD patters of the tri-component catalysts totally changed and showed a similar tendency except for Ce1Sn2. The peaks belonging to the TiO_2 disappeared completely while no distinctively obvious diffraction peaks of CeO_2 or SnO_2 appeared. We deduced that it was the synergistic effect existing among the mixed oxides in the tri-components catalyst hindered the crystal phase formation of TiO_2 [32]. Only a very broad and weak peak was observed at the range $2\theta = 20–40°$ in Fig. 5(b), suggesting the samples were in poor crystallization. From the low intensity of this special X-ray diffraction characteristic peak, it could be declared that all metal components are highly dispersed and inherently amorphous in structure because of the introduction of Sn, which was beneficial to obtain excellent SCR catalytic activity, accompanied with the higher BET specific surface area. Besides, the peak became more evident with the increase of Sn content, implying that the introduction of moderate Sn might result in a stronger interaction between cerium and titanium [23]. However, it was worth noticed that the accretion of redundant SnO_2 on CeTi resulted in the appearance of new diffraction peaks obviously identified in Ce1Sn2, which belonged to the diffraction characteristic peaks of Ti–Sn mixed oxides [38]. The reason might be that excess Sn promoted the crystal phase of TiO_2 to form a rutile structure and the peak position gradually shifted to lower angle with the increase of SnO_2 compared with SnTi.

In order to ascertain the synergistic effect of SnO_2 on the tri-components catalyst Ce2Sn1, Raman spectroscope was employed to detect the surface information of the catalyst, as a potential complementary characterization of XRD. For comparison, Raman spectroscope was also performed on the bi-components catalyst CeTi. Fig. 6 showed the corresponding results of Raman spectroscope ranging from 100 to 1000 cm^{-1}. The bi-components catalyst revealed four typical Raman bands due to the anatase TiO_2, which were located at about 149, 399, 519 and 645 cm^{-1}. According to the literature, the strong peak at 149 cm^{-1} is attributed to the bending vibration mode of O—Ti—O and the other three faintish bands are assigned to the symmetric bending vibration of O—Ti—O, the unsymmetrical bending vibration of O—Ti—O and the symmetric stretching vibration of O—Ti—O, respectively [13]. After Sn was further introduced, the typical peaks of TiO_2 at 147 cm^{-1} and 517 cm^{-1} became weaker and shifted to lower-wavenumber direction slightly, while the peaks at 399 cm^{-1} and 645 cm^{-1} disappeared completely. It is apparently promulgated that the addition of SnO_2 strongly inhibited the crystallization of anatase TiO_2 on the surface of the tri-components catalyst Ce2Sn1, further indicating that the introduction of SnO_2 might enhance the interaction

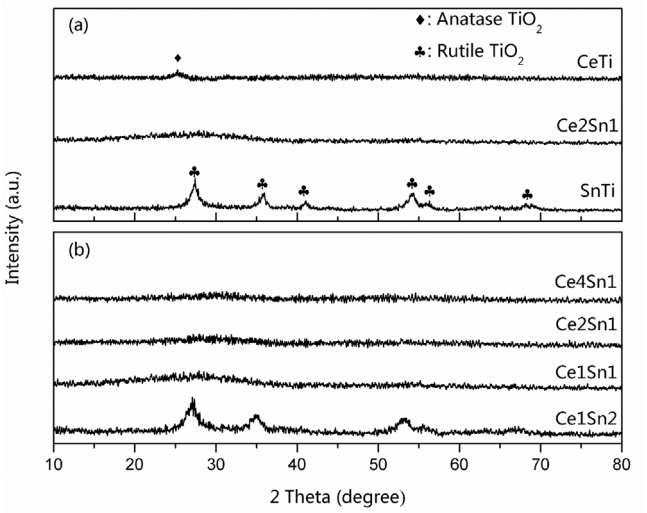

Fig. 5. XRD patterns of: (a) Ce–Sn–Ti dual component oxide catalysts; (b) different Ce*x*Sn*y* catalysts.

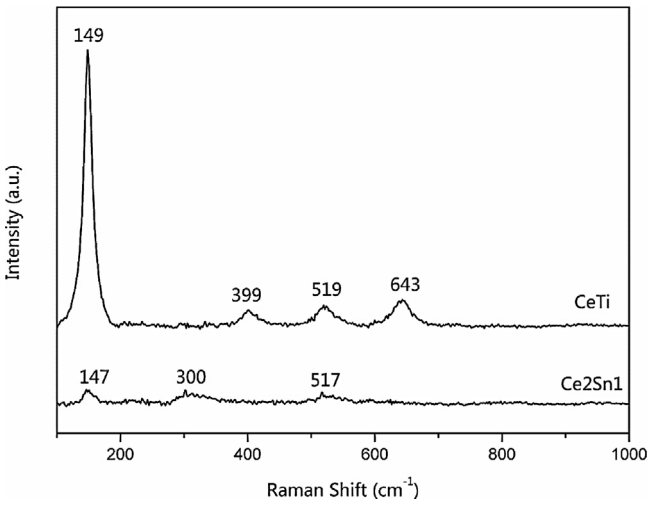

Fig. 6. Raman spectra of CeTi and Ce2Sn1 catalysts at 100–1000 cm^{-1}.

Table 2
The surface compositions of the samples obtained by XPS analysis.

Samples	Atomic concentration (at.%)				Atomic ratio (%)		
	Ce	Sn	Ti	O	$Ce^{3+}/(Ce^{3+}+Ce^{4+})$	O/(Ce + Sn + Ti)	$O_\alpha/(O_\alpha+O_\beta)$
SnTi	–	5.79	23.58	70.63	–	2.40 (2.00)	17.73
CeTi	5.01	–	23.29	71.69	23.37	2.53 (2.00)	46.71
Ce2Sn1	5.36	4.27	21.41	68.96	29.62	2.22 (2.00)	57.89

between titanium and ceria. Similar to the above XRD results, the Raman band at 464 cm^{-1} corresponding to the F_{2g} vibration mode of cubic fluorite-type structure was absent in both of the two catalysts, declaring the preferable dispersion degree of Ce on surfaces of the two catalysts and likewise, no bands belonging to SnO_2 were found in the tri-components catalyst. Besides, it was noteworthy that there was a new and weak band at 300 cm^{-1} in the tri-components catalyst, which is linked to the presence of oxygen vacancies ($V_O^{\bullet}$) in CeO_2 lattice [39]. This phenomenon implied that the doping of SnO_2 could increase extra oxygen vacancy to some degree, the generation of which can enhance the redox ability of the tri-components catalyst and further facilitate NO oxidation to NO_2, contributing to improving the catalytic performance at low temperature via a fast SCR reaction: $2NH_3 + NO + NO_2 \rightarrow 2N_2 + 3H_2O$ [40]. In such case, it is reasonable to discover that the tri-components catalyst showed a better catalytic efficiency than the bi-components catalyst through the introduction of SnO_2.

3.2.2. Surface chemical states (XPS)

XPS was employed to characterize the elementary oxidation states and the surface compositions of these synthesized samples. The surface atomic concentrations of all the elements were summarized in Table 2, and different XPS spectra of Ti 2p, Ce 3d, Sn 3d, and O 1s were presented in Figs. 7–10.

It can be seen from Fig. 7 that the binding energies of Ti 2p photoelectron peaks in the bi-components catalysts were about 458.7 and 464.3 eV, representing Ti 2p3/2 and Ti 2p1/2 respectively. This indicated that Ti existed in the Ti^{4+} oxidation state in a tetragonal structure, instead of Ti^{3+}, in the bi-components catalysts [36,41]. Researchers have reported that when an extraneous metal was added into TiO_2, the binding energy of the Ti 2p peaks slightly shifted to higher binding energy than that of pure Ti 2p, owing to the metal–support interaction effect generated between the mixed oxides [42]. In this study, after the addition of Ce or Sn into TiO_2, the binding energies shifted slightly to higher values, in well accordance with the literature. Moreover, a slightly increase in binding

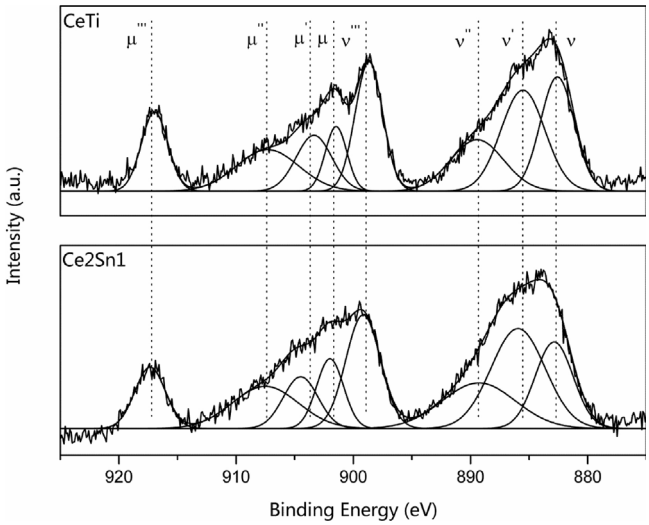

Fig. 8. Ce_{3d} spectra for CeTi and Ce2Sn1 catalysts.

energies of the tri-components catalyst Ce2Sn1 was observed with Ti^{4+} 2p3/2 shifting to 458.9 eV and Ti^{4+} 2p1/2 shifting to 464.5 eV. The blue-shift in the binding energies implied that the titanium species in the tri-components catalyst had lower density of electron cloud around Ti atoms than that in the bi-components catalysts, which further indicating the stronger interaction among the metal oxides, as shown in the previous XRD [6,43].

The optimum combination of Gaussian fitting bandsman of Ce 3d for different catalysts are depicted in Fig. 8 with the correlation coefficients (r^2) above 0.99. The complex peaks were decomposed into eight components. According to the literature, the sub-bands labeled u' and v' are related to the $3d^{10}4f^1$ initial electronic state corresponding to Ce^{3+}, while the other six sub-bands labeled u and v, u'' and v'', u''' and v''' represent the $3d^{10}4f^0$ state of Ce^{4+} ions [44]. It was apparent to observe that Ce^{4+} oxidation state was the

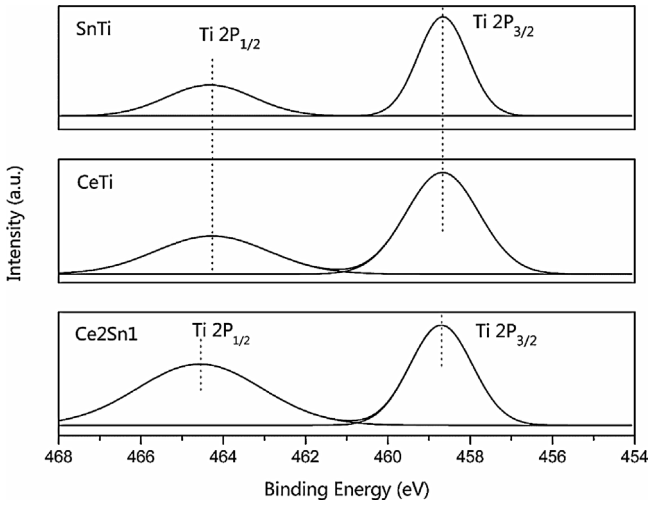

Fig. 7. Ti_{2p} spectra for SnTi, CeTi and Ce2Sn1 catalysts.

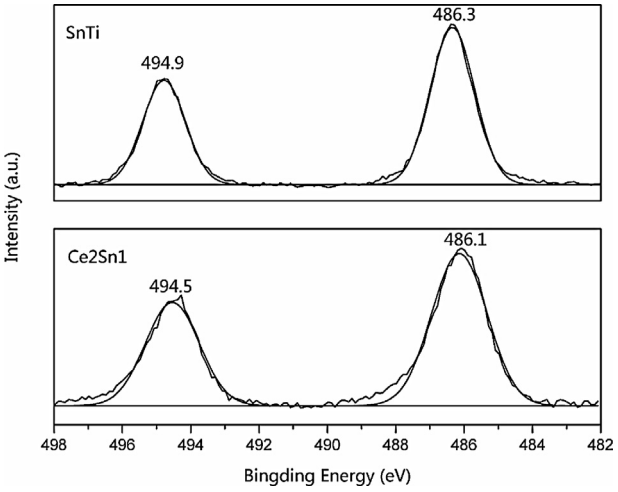

Fig. 9. Sn_{3d} spectra for SnTi and Ce2Sn1 catalysts.

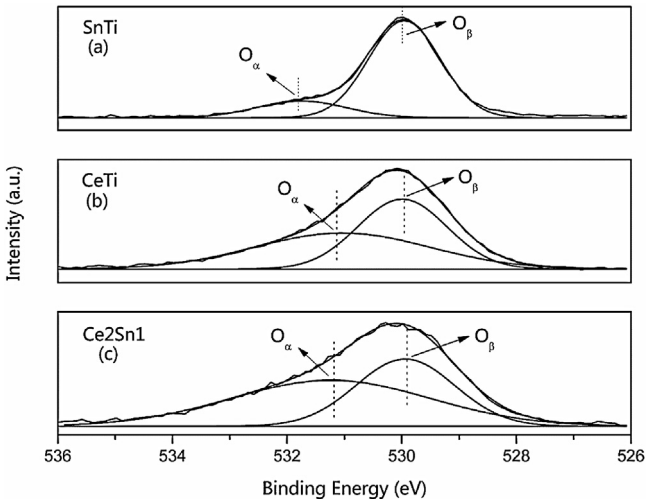

Fig. 10. O_{1s} spectra for SnTi, CeTi and Ce2Sn1 catalysts.

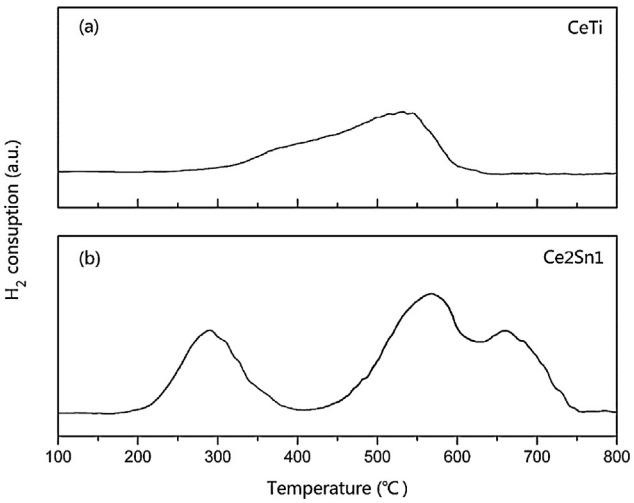

Fig. 11. H_2-TPR profiles of CeTi (a) and Ce2Sn1 (b).

preponderantly chemical valence on the surface of the bi-components catalyst, which hint that the catalyst surface were not fully oxidized, and this situation also happened in the tri-components catalyst. The typical redox couple Ce^{4+}/Ce^{3+} could function well together to achieve high catalytic efficiency by producing labile oxygen vacancies and highly mobile oxygen during the process of the redox shift [45,46]. It is a consensus that the presence of more Ce^{3+} is beneficial to the SCR reaction because Ce^{3+} could create a charge balance, form oxygen vacancies and unsaturated chemical bond on the catalysts surface, which will lead to an increase of chemisorbed oxygen [47]. Accordingly, the Ce^{3+} contents of the catalysts can be determined by calculating the area ratio of these bands based on the following equation: $Ce^{3+}(\%) = S_{\mu'} + S_{\nu'} / \sum(S_\mu + S_\nu) \times 100$ and the results were listed in Table 2. It can be seen from Table 2 that the Ce^{3+} concentration of the tri-components catalyst (29.62%) was higher than that of the bi-components catalyst (23.37%). Therefore, it is most likely that the introduction of Sn contributed to the transformation from Ce^{4+} to Ce^{3+} ions, which could create a charge imbalance, the vacancies and unsaturated chemical bonds over the catalyst surface, and more NO could be easily oxides into NO_2, partially accounting for the better SCR catalytic efficacy of the tri-components catalyst than that of the bi-components catalyst. There are two possible reasons: the first reason is that the addition of Sn enhanced the interaction among the mixed oxides to increase the contents of Ce^{3+}, which is supported by the XRD results, following the reaction $Ti^{3+} + Ce^{4+} \leftrightarrow Ti^{4+} + Ce^{3+}$ and $2Ce^{4+} + Sn^{2+} \leftrightarrow 2Ce^{3+} + Sn^{4+}$, and the second reason is that the electrons of oxygen vacancies were captured by Ce^{4+} to form Ce^{3+} because of the electron-donating effects, following the reaction $V_O^{\bullet} + Ce^{4+} \leftrightarrow Ce^{3+} + V_O$.

The spectrum of Sn 3d of Ce2Sn1 and SnTi are numerically fitted with two components, as shown in Fig. 9. For SnTi, the binding energies of Sn 3d5/2 and Sn 3d3/2 of SnO_2 were located at 486.3 and 494.9 eV respectively. In the case of Ce2Sn1, the Sn 3d5/2 and Sn 3d3/2 peaks appeared at 486.1 and 494.5 eV. The lower, weaker and broader peaks indicated that there existed excess electrons around Sn in Ce2Sn1, further elucidating the existence of synergistic interaction among the mixed oxides through the redox equilibrium of $2Ce^{4+} + Sn^{2+} \leftrightarrow 2Ce^{3+} + Sn^{4+}$ [48].

The XPS spectrum for O 1s ionization features of all these samples is numerically fitted into two sub-bands by searching for the optimal combination of Gaussian bands, and the corresponding assignments are defined in Fig. 10. The higher banding energy of 531.0–531.6 eV is considered as the chemisorbed oxygen or weakly bonded oxygen species (donated as O_α), such as O_2^{2-} or O^- in defect-oxide or hydroxyl-like groups, whereas the lower binding energy of 529.2–530.0 eV is the characteristic lattice oxygen bonding to the metal cations (donated as O_β) [39]. As shown in Table 2, the ratio of $O_\alpha/(O_\alpha + O_\beta)$ in all the catalysts were calculated based on the area integral of O_α and O_β. We can see from Table 2 that the relative concentration ratio of O_α increased in the following sequence: Ce2Sn1 (57.89%) > CeTi (46.71%) > SnTi (17.73%), which was in corresponding with the trend of the SCR catalytic activity. Many researchers have proposed that chemisorbed oxygen O_α was more active than lattice oxygen in oxidation reactions and plays an important role in oxidation reaction because of its higher mobility [18,20]. In consequence, the higher O_α ratio in Ce2Sn1 would contribute to nitric adsorption by facilitating the oxidation of NO to NO_2 in the SCR reaction, which agreed with the Raman results. Considering the higher content of Ce^{3+} in Ce2Sn1, the occurrence of more O_α is by no means fortuitous since Ce^{3+} is a fabricant of surface chemisorbed oxygen, which generated by the redox cycle Ce^{4+}/Ce^{3+}. Besides, it can be seen from Table 2 that the atomic ration of O/(Ce + Sn + Ti) for each catalysts is higher than its theoretic value (2.00) in the full oxidation states, demonstrating the chemisorbed oxygen of surface water or hydroxyl on the surface of the samples [49].

3.2.3. *Reduction properties (H_2-TPR)*

The redox properties are the key factors determining the reactivity of NH_3-SCR catalysts. In order to figure out the effect of SnO_2 on the redox ability of CeTi, H_2-TPR was employed as an extensively used technique to estimate the redox properties of the catalysts and the obtained profiles were shown in Fig. 11. We can see from Fig. 11(a) that the CeTi catalyst possessed an overlapped reduction peak from 400 to 600 °C, which is indeed very similar to the reduction behavior observed in other report [46,50]. According to the literature, the wide ranged peak could be interpreted as a stepwise reduction: the first step is due to the reduction of surface oxygen of stoichiometric ceria (Ce^{4+}–O–Ce^{4+}) and the second step is attributed to the reduction of non-stoichiometric ceria (Ce^{3+}–O–Ce^{4+}) [51]. An addition of SnO_2 to the CeTi catalyst produced a new peak of oxygen species, which can be reduced by hydrogen in a lower temperature around 290 °C. Baidya et al. has previously concluded that the reduction peaks in $Ce_{0.6}Sn_{0.4}O_2$ before 550 °C was duo to the reduction of Sn^{4+} to the Sn^{2+} state and partial reduction of Ce^{4+} to the Ce^{3+} state [52]. Accordingly, in this work, the novel peak appearing at lower temperatures may originate from the interaction between Ce^{4+}/Ce^{3+} and Sn^{4+}/Sn^{2+} through the redox equilibrium of $2Ce^{4+} + Sn^{2+} \leftrightarrow 2Ce^{3+} + Sn^{4+}$,

indicating that the oxygen atoms of Ce2Sn1 are easier migrate to generate oxygen vacancy during the reduction process in lower temperature. In addition, Chen et al. reported that SnO_2 exhibited a major reduction peak at about 670 °C and the final product was Sn^0 mental [53]. Therefore, we supposed that the reduction peak above 550 °C may be attributed to the reduction of Sn^{4+} to the Sn^0 and the reduction of bulk CeO_2.

Moreover, integral areas of the H_2-TPR profiles were usually calculated to compare the oxygen storage capacity of catalysts, which is a significant parameter to the SCR activity of ceria-based catalysts. The higher total H_2 consumption obtained from the obviously larger peak area of Ce2Sn1 than that of CeTi implied that the introduction of SnO_2 resulted in more reducible subsurface and bulk oxygen in the tri-components catalyst, which is responsible for the better SCR catalytic performance of Ce2Sn1.

3.2.4. Possible reaction mechanism over Ce2Sn1

For NH_3-SCR process, the mechanism has been extensively studied. Different hypotheses have been proposed for the mechanisms over different catalysts, involving both the Eley–Rideal (E–R) mechanism and Langmuir–Hinshelwood (L–H) mechanism. Li et al. proposed a simplified reaction mechanism on CeTi catalyst on the basis of in situ diffuse reflectance infrared transform spectroscopy [54]. On one hand, the L–H mechanism was suggested at temperature lower than 200 °C, which could take place between the coordinated NH_3 and adsorbed NO_3^- species:

$$O_2(g) \rightarrow 2O \quad (2)$$

$$NO(g) + O \rightarrow NO_2(a) \quad (3)$$

$$2NH_3(a) + NO_2(a) + NO \rightarrow 2N_2 + 3H_2O \quad (4)$$

Liu et al. indicated that the formation of adsorbed NO_3^- species was actually the rate-determining step for the L–H mechanism on FeTi catalyst because it could be consumed quickly to produce the final products, which was also appropriate for CeTi [55]. Canevali indicated that the interaction of NO with SnO_2 involves electron injection of NO to SnO_2, formation of oxygen vacancies and chemisorption of NO_3^- species [56]. Hence, the addition of SnO_2 over CeTi catalyst could generate more adsorbed NO_3^- species, thus enhancing the SCR reaction through the L–H mechanism.

On the other hand, E–R mechanism might become the main reaction pathway at temperature higher than 200 °C, which was proposed as that NH_3 was firstly adsorbed on the catalyst after the competitive adsorption, and then the formed amide species reacted with the gaseous NO to generate the intermediate NH_2NO. Because of the low thermal stability, NH_2NO could decompose into N_2 and H_2O rapidly:

$$NH_3(a) \rightarrow NH_2(a) + H^+ + e^- \quad (5)$$

$$NH_2(a) + NO(g) \rightarrow NH_2NO(a) \rightarrow N_2 + H_2O \quad (6)$$

Liu et al. proved that the formation of NH_2NO was the actual rate-determining step in the overall SCR reaction [55]. According to the literature, NH_3 can be favorably chemically adsorbed on the surface of SnO_2 to form NH_2 species through the strong acidity of Sn^{4+} [56]. Therefore, the addition of SnO_2 over CeTi catalyst could enhance the NH_3 adsorption ability and brought more active NH_3 adsorbed species, further facilitating the SCR reaction through E–R mechanism. During this process, Ce^{4+} and Sn^{4+} was firstly reduced to Ce^{3+} and Sn^{2+} respectively in the H-abstraction step of coordinated NH_3, and then oxidized by O_2 to their original oxidization state to complete a redox circle.

Furthermore, the synergistic effect between CeO_2 and SnO_2 might exist in the form of $2Ce^{4+} + Sn^{2+} \leftrightarrow 2Ce^{3+} + Sn^{4+}$, according to the results of XRD, Raman, XPS and H_2-TPR. The electron transferring phenomenon could further enhance the NO oxidation reaction shown in equation 7–9 via the following reactions [57]:

$$Ce^{3+} + O_2 \rightarrow Ce^{4+} + 2O^-(a) \quad (7)$$

$$Sn^{4+} + 2NO \rightarrow Sn^{2+} + 2NO^+(a) \quad (8)$$

$$NO^+(a) + O^-(a) \rightarrow NO_2 \quad (9)$$

4. Conclusions

All the catalysts were synthesized by the inverse co-precipitation method and tested for the catalytic performance. The introduction of SnO_2 to CeTi contributed a higher NO removal efficiency and the optimal value of the molar ratio of Ce: Sn was 2:1. Satisfied NO removal efficiency can be achieved at low temperature, while over 90% NO conversion was maintained at the gas hourly space velocity of 50,000 h^{-1} over the Ce2Sn1 catalyst. Meanwhile, Ce2Sn1 kept a stable NO removal efficiency within a wide range of GHSV and a long period of reacting time. In addition, Ce2Sn1 possessed remarkable resistance to both respectively and simultaneously water and sulfur.

The promotional effect of SnO_2 was confirmed by a serious of characterizations. The results of BET, XRD and Raman revealed that the superior performance of Ce2Sn1 was attributed to better structure properties, such as the highest specific surface area and largest pore volume, the poor crystallization and the strong interaction among the mixed oxides. Through XPS analysis, the introduction of SnO_2 resulted in not only the present of more Ce^{3+} through $Ti^{3+} + Ce^{4+} \leftrightarrow Ti^{4+} + Ce^{3+}$ and $2Ce^{4+} + Sn^{2+} \leftrightarrow 2Ce^{3+} + Sn^{4+}$, but also the increase amount of chemisorbed oxygen or weakly bonded oxygen species (O_α), which played an essential role in catalytic performance. Besides, more efficient redox ability was obtained in Ce2Sn1, proved by a novel peak appearing at lower temperatures through the new redox equilibrium of $2Ce^{4+} + Sn^{2+} \leftrightarrow 2Ce^{3+} + Sn^{4+}$ and higher total H_2 consumption. All the advantages above resulted in the superior performance of Ce2Sn1. Finally, the possible reaction mechanism of selective catalytic reduction over Ce2Sn1 was also discussed. The introduction of SnO_2 could contribute to the SCR activity via both the Eley–Rideal (E–R) mechanism and Langmuir–Hinshelwood (L–H) mechanism. The electron transfer between Ce^{3+} and Sn^{4+} was also beneficial to the SCR activity to some extent. Finally, more details about the reaction mechanism of Ce2Sn1 will be studied further in the future.

Acknowledgement

This project is financially supported by the National Natural Science Foundation of China (51278177, 51478173).

References

[1] H. Bosh, F.J. Janssen, Formation and control of nitrogen oxides, Catal. Today 2 (1988) 369–379.
[2] G. Busca, L. Liette, G. Ramis, Chemical and mechanistic aspects of the selective catalytic reduction of NO_x by ammonia over oxide catalysts: a review, Appl. Catal. B: Environ. 18 (1998) 1–36.
[3] P. Forzatti, Environmental catalysis for stationary applications, Catal. Today 62 (2000) 51–65.
[4] Y.P. Zhang, X.Q. Zhu, K. Shen, H.T. Xu, K.Q. Sun, C.C. Zhou, Influence of ceria modification on the properties of TiO_2–ZrO_2 supported V_2O_5 catalysts for selective catalytic reduction of NO by NH_3, J. Colloid Interface Sci. 376 (2012) 233–238.
[5] S.M. Lee, K.H. Park, S.C. Hong, MnO_x/CeO_2–TiO_2 mixed oxide catalysts for the selective catalytic reduction of NO with NH_3 at low temperature, Chem. Eng. J. 195 (2012) 323–331.
[6] S.L. Zhang, Q. Zhong, Promotional effect of WO_3 on O_2^- over V_2O_5/TiO_2 catalyst for selective catalytic reduction of NO with NH_3, J. Mol. Catal. A: Chem. 373 (2013) 108–113.
[7] S. Djerad, M. Crocoll, S. Kureti, L. Tifouti, W. Weisweiler, Effect of oxygen concentration on the NO_x reduction with ammonia over V_2O_5–WO_3/TiO_2 catalyst, Catal. Today 113 (2006) 208–214.

[8] J.P. Dunn, P.R. Koppula, H.G. Stenger, I.E. Watchs, Oxidation of sulfur dioxide to sulfur trioxide over supported vanadium catalysts, Appl. Catal. B: Environ. 19 (1998) 103–117.

[9] L. Qu, C.T. Li, G.M. Zeng, M.Y. Zhang, M.F. Fu, J.F. Ma, F.M. Zhan, D.Q. Luo, Support modification for improving the performance of MnO_x–CeO_y/γ-Al_2O_3 in selective catalytic reduction of NO by NH_3, Chem. Eng. J. 242 (2014) 76–85.

[10] M.Y. Zhang, C.T. Li, L. Qu, M.F. Fu, G.M. Zeng, J.F. Ma, C.Z. Fang, F.M. Zhan, Catalytic oxidation of NO with O_2 over $FeMnO_x$/TiO_2: effect of iron and manganese oxides loading sequences and the catalytic mechanism study, Appl. Surf. Sci. 300 (2014) 58–65.

[11] Z.X. Ma, H. Sh Yang, Q. Li, J.W. Zheng, X.B. Zhang, Catalytic reduction of NO by NH_3 over Fe–Cu–O_x/CNTs–TiO_2 composites at low temperature, Appl. Catal. A: Gen. 427–428 (2012) 43–48.

[12] R.Y. Qu, X. Gao, K.F. Cen, J.H. Li, Relationship between structure and performance of a novel cerium-niobium binary oxide catalyst for selective catalytic reduction of NO with NH_3, Appl. Catal. B: Environ. 142–143 (2013) 290–297.

[13] Z.M. Liu, Y. Yi, J.H. Li, S.I. Woo, B.Y. Wang, X.Z. Cao, Z.X. Li, A superior catalyst with dual redox cycles for the selective reduction of NO_x by ammonia, Chem. Commun. 49 (2013) 7726–7728.

[14] L.L. Zhu, B.C. Huang, W.H. Wang, Low-temperature SCR of NO with NH_3 over CeO_2 supported on modified activated carbon fibers, Catal. Commun. 12 (2011) 394–398.

[15] Y.S. Shen, S.M. Zhu, T. Qiu, A novel catalyst of CeO_2/Al_2O_3 for selective catalytic reduction of NO by NH_3, Catal. Commun. 11 (2009) 20–23.

[16] G.S. Qi, R.T. Yang, R. Chang, MnO_x–CeO_2 mixed oxides prepared by co-precipitation for selective catalytic reduction of NO with NH_3 at low temperatures, Appl. Catal. B: Environ. 51 (2004) 93–106.

[17] Y. Peng, C.Z. Wang, J.H. Li, Structure–activity relationship of VO_x/CeO_2 nanorod for NO removal with ammonia, Appl. Catal. B: Environ. 144 (2014) 538–546.

[18] X. Gao, Y. Jiang, Y. Zhong, Z.Y. Luo, K.F. Cen, The activity and characterization of CeO_2–TiO_2 catalysts prepared by the sol–gel method for selective catalytic reduction of NO with NH_3, J. Hazard. Mater. 174 (2010) 734–739.

[19] X. Gao, Y. Jiang, Y.C. Fu, Y. Zhong, Z.Y. Luo, K.F. Cen, Preparation and characterization of CeO_2/TiO_2catalysts for selective catalytic reduction of NO with NH_3, Catal. Commun. 11 (2010) 465–469.

[20] W.P. Shan, F.D. Liu, H. He, X.Y. Shi, C.B. Zh, An environmentally benign CeO_2–TiO_2 catalyst for the selective catalytic reduction of NO_x with NH_3 in simulated diesel exhaust, Catal. Today 184 (2012) 160–165.

[21] W.P. Sh, F.D. Liu, H. He, X.Y. Shi, C.B. Zh, A superior Ce–W–Ti mixed oxide catalyst for the selective catalytic reduction of NO_x with NH_3, Appl. Catal. B: Environ. 115–116 (2012) 100–106.

[22] Z.M. Liu, S.X. Zhang, J.H. Li, L.L. Ma, Promoting effect of MoO_3 on the NO_x reduction by NH_3 over CeO_2/TiO_2 catalyst studied with in situ DRIFTS, Appl. Catal. B: Environ. 144 (2014) 90–95.

[23] R. Zhang, Q. Zhong, W. Zhao, L.M. Yu, H.X. Qu, Promotional effect of fluorine on the selective catalytic reduction of NO with NH_3 over CeO_2–TiO_2 catalyst at low temperature, Appl. Surf. Sci. 289 (2014) 237–244.

[24] A. Iglesias-González, J.L. Ayastuy, M.P. González-Marcos, M.A. Gutiérrez-Ortiz, CuO/$Ce_xSn_{1-x}O_2$ catalysts with low tin content for CO removal from H_2-rich streams, Int. J. Hydrogen Energy 10 (2014) 5213–5224.

[25] B. Mirkelamoglu, G. Karakas, CO oxidation over palladium and sodium-promoted tin dioxide: catalyst characterization and temperature-programmed studies, Appl. Catal. A: Gen. 281 (2005) 275–284.

[26] D.F. Cox, T.B. Fryberge, S. Semancik, Oxygen vacancies and defect electronic states on the SnO_2 (1 1 0)-1 × 1 surface, Phys. Rev. B 38 (3) (1998) 2072–2082.

[27] X.L. Li, Y.H. Li, S.S. Deng, T.A. Rong, A Ce–Sn–O_x catalyst for the selective catalytic reduction of NO_x with NH_3, Catal. Commun. 40 (2013) 47–50.

[28] H.Z. Chang, J.H. Li, X.Y. Chen, L. Ma, S.J. Yang, J.W. Schwank, J.M. Hao, Effect of Sn on MnO_x–CeO_2 catalysts for SCR of NO_x by ammonia: enhancement of activity and remarkable resistance to SO_2, Catal. Commun. 27 (2012) 54–57.

[29] H.Z. Chang, X.Y. Chen, J.H. Li, L. Ma, Improvement of activity and SO_2 tolerance of Sn-modified MnO_x–CeO_2 catalysts for NH_3-SCR at low temperatures, Environ. Sci. Technol. 47 (2013) 5294–5301.

[30] B. Jiang, Z. Wu, Y. Liu, Low-temperature selective catalytic reduction of NO on MnO_x/TiO_2 prepared by different methods, J. Hazard. Mater. 145 (2009) 1249–1254.

[31] W.Q. Xu, H. He, Y.B. Yu, Deactivation of a Ce/TiO_2 catalyst by SO_2 in the selective catalytic reduction of NO by NH_3, J. Phys. Chem. C 113 (2009) 4426–4432.

[32] C.X. Liu, L. Ch, J.H. Li, L. Ma, H. Arandiam, Y. Du, J.Y. Xu, J.M. Hao, Enhancement of activity and sulfur resistance of CeO_2 supported on TiO_2–SiO_2 for the selective catalytic reduction of NO by NH_3, Environ. Sci. Technol. 46 (2012) 6128–6189.

[33] D. Yuan, X. Li, Q. Zhao, J. Zhao, S. Liu, M. Tadé, Effect of surface Lewis acidity on selective catalytic reduction of NO by C_3H_6 over calcined hydrotalcite, Appl. Catal. A: Gen. 451 (2013) 176–183.

[34] J.G. Yu, Q.J. Xiang, J.R. Ran, S. Mann, One-step hydrothermal fabrication and photocatalytic activity of surface-fluorinated TiO_2 hollow microspheres and tabular anatase single micro-crystals with high-energy facets, Cryst. Eng. Commun. 12 (2010) 872–879.

[35] J. Fang, H.Z. Bao, B. He, F. Wang, D.J. Si, Z.Q. Jiang, Z.Y. Pan, S.Q. Wei, W.X. Huang, Interfacial and surface structure of CeO_2–TiO_2 mixed oxides, J. Phys. Chem. C 11 (2007) 19078–19085.

[36] J. Fang, X.Z. Bi, D.J. Si, Z.Q. Jiang, W.X. Huang, Spectroscopic studies of interfacial structures of CeO_2–TiO_2 mixed oxides, Appl. Surf. Sci. 253 (2007) 8952–8961.

[37] P. Li, Y. Xin, Q. Li, Z.P. Wang, Z.L. Zhang, L.R. Zheng, Ce–Ti amorphous oxides for selective catalytic reduction of NO with NH_3: confirmation of Ce–O–Ti active sites, Environ. Sci. Technol. 46 (2012) 9600–9605.

[38] L.H. Dong, C.Z. Sun, C.J. Tang, B. Zhang, J. Zhu, B. Liu, F. Gao, Y.H. Hua, L. Dong, Y. Chen, Investigations of surface VO_x species and their contributions to activities of VO_x/$Ti_{0.5}$–$Sn_{0.5}O_2$ catalysts toward selective catalytic reduction of NO by NH_3, Appl. Catal. A: Gen. 431–432 (2012) 126–136.

[39] D.R. Sellick, A. Aranda, T. García, J.M. López, B. Solsona, A.M. Mastral, D.J. Morgan, A.F. Carley, S.H. Taylor, Influence of the preparation method on the activity of ceria zirconia mixed oxides for naphthalene total oxidation, Appl. Catal. B: Environ. 132–133 (2013) 98–106.

[40] C. Ciardelli, I. Nova, E. Tronconi, D. Chatterjee, B. BandlKonrad, A "Nitrate Route" for the low temperature "Fast SCR" reaction over a V_2O_5–WO_3/TiO_2 commercial catalyst, Chem. Commun. 23 (2004) 2718–2719.

[41] T. Gu, R. Jin, Y. Liu, H. Liu, X. Weng, Z. Wu, Promoting effect of calcium doping on the performances of MnO_x/TiO_2 catalysts for NO reduction with NH_3 at low temperature, Appl. Catal. B: Environ. 129 (2013) 30–38.

[42] S.M. Lee, H.H. Lee, S.C. Hong, Influence of calcination temperature on Ce/TiO_2 catalysis of selective catalytic oxidation of NH_3 to N_2, Appl. Catal. A: Gen. 470 (2014) 189–198.

[43] S.L. Zhang, H.Y. Li, Q. Zhong, Promotional effect of F-doped V_2O_5–WO_3/TiO_2 catalyst for NH_3-SCR of NO at low-temperature, Appl. Catal. A: Gen. 435–436 (2012) 156–162.

[44] V.M. Shinde, G. Madras, Synthesis of nanosized $Ce_{0.85}M_{0.1}Ru_{0.05}O_{2-\delta}$ (M = Si, Fe) solid solution exhibiting high CO oxidation and water gas shift activity, Appl. Catal. B: Environ. 138–139 (2013) 51–61.

[45] B.M. Reddy, A. Khan, Y. Yamada, T. Kobayashi, S. Loridant, J.C. Volta, Structural characterization of CeO_2–TiO_2 and V_2O_5/CeO_2–TiO_2 catalysts by Raman and XPS techniques, J. Phys. Chem. B 107 (2003) 5162–5167.

[46] J. Fang, H.Z. Bao, K. Qian, Z.Q. Jiang, W.X. Huang, Evolution of surface and bulk structures of $Ce_xTi_{1-x}O_2$ oxide composites, Chin. J. Catal. 34 (2013) 2075–2083.

[47] H.Q. Wang, X.B. Chen, S. Gao, Z.B. Wu, Y. Liu, X.L. Weng, Deactivation mechanism of Ce/TiO_2 selective catalytic reduction catalysts by the loading of sodium and calcium salts, Catal. Sci. Technol. 3 (3) (2013) 715–722.

[48] X.J. Yao, Y. Xiong, W.X. Zou, L. Zhang, Correlation between the physicochemical properties and catalytic performances of $Ce_xSn_{1-x}O_2$ mixed oxides for NO reduction by CO, Appl. Catal. B: Environ. 144 (2014) 152–165.

[49] X.J. Yao, L. Zhang, L.L. Li, L.C. Liu, Investigation of the structure, acidity, and catalytic performance of CuO/$Ti_{0.95}Ce_{0.05}O_2$ catalyst for the selective catalytic reduction of NO by NH_3 at low temperature, Appl. Catal. B: Environ. 150–151 (2014) 315–329.

[50] X.J. Yao, C.J. Tang, Z.Y. Ji, Y. Dai, Y. Cao, F. Gao, L. Dong, Y. Chen, Investigation of the physicochemical properties and catalytic activities of $Ce_{0.67}M_{0.33}O_2$ (M = Zr^{4+}, Ti^{4+}, Sn^{4+}) solid solutions for NO removal by CO, Catal. Sci. Technol. 3 (2013) 688–698.

[51] B. Murugan, A.V. Ramaswamy, Chemical states and redox properties of Mn/CeO_2−TiO_2 nanocomposites prepared by solution combustion route, J. Phys. Chem. C 112 (2008) 20429–20442.

[52] T. Baidya, A. Gupta, P.A. Deshpandey, G. Madras, M.S. Hegde, High oxygen storage capacity and high rates of CO oxidation and NO reduction catalytic properties of $Ce_{1-x}Sn_xO_2$ and $Ce_{0.78}Sn_{0.2}Pd_{0.02}O_{2-\delta}$, J. Phys. Chem. C 113 (2009) 4059–4068.

[53] Y.Z. Chen, B.J. Liaw, C.W. Huang, Selective oxidation of CO in excess hydrogen over CuO/$Ce_xSn_{1-x}O_2$ catalysts, Appl. Catal. A: Gen. 302 (2006) 168–176.

[54] L. Chen, J.H. Li, M.F. Ge, DRIFT study on cerium–tungsten/titiania catalyst for selective catalytic reduction of NO_x with NH_3, Environ. Sci. Technol. 44 (2010) 9590–9596.

[55] F.D. Liu, H. He, C.B. Zhang, W.P. Shan, X.Y. Shi, Mechanism of the selective catalytic reduction of NO_x with NH_3 over environmental-friendly iron titanate catalyst, Catal. Today 175 (2011) 18–25.

[56] C. Canevali, C.M. Mari, M. Mattoni, F. Morazzoni, R. Ruffo, R. Scotti, U. Russo, L. Nodarib, Mechanism of sensing NO in argon by nanocrystalline SnO_2: electron paramagnetic resonance, Mössbauer and electrical study, Sens. Actuators B 100 (2004) 228–235.

[57] M.W. Abee, D.F. Cox, NH_3 chemisorption on stoichiometric and oxygen-deficient SnO_2 (1 1 0) surfaces, Surf. Sci. 520 (2002) 65–77.